Research Square

Preprints are preliminary reports that have not undergone peer review.
They should not be considered conclusive, used to inform clinical practice,
or referenced by the media as validated information.

Climate impacts of transitioning shipping fuel

Homa Esfandiari

homa.esfandiari@ntnu.no

Norwegian University of Science and Technology

Diogo Kramel

Norwegian University of Science and Technology

Helene Muri

NILU

Article

Keywords: Shipping, Decarbonization, Fuel transition, Earth system modelling

Posted Date: November 17th, 2026

DOI: https://doi.org/10.21203/rs.3.rs-11626954/v1

License: This work is licensed under a Creative Commons Attribution 4.0 International License.
Read Full License

Additional Declarations: No competing interests reported.

Climate impacts of transitioning shipping fuel

Homa Esfandiari*[1], Diogo Kramel[1], Helene Muri*[1,2]

[1]Department of Energy and Process Engineering, Norwegian University of Science and Technology (NTNU), Trondheim, Norway

[2]Department of Atmosphere and Climate, NILU, Kjeller, Norway

* Corresponding authors: helene.muri@ntnu.no; homa.esfandiari@ntnu.no

Abstract

Switching marine fuels reduces carbon emissions while altering the short-lived atmospheric species that influence climate change. Here we assess such effects by running Earth system model simulations with globally resolved well-to-wake shipping emission as input. Comparing global shipping run on very-low-sulfur fuel oil, high-pressure liquefied natural gas, and blue ammonia with 2019 marine fuel mix, all alternatives reduce global sulfate burden most strongly along Northern Hemisphere shipping corridors and downwind continental regions; LNG and blue ammonia additionally reduce black carbon. Reduced aerosol availability leads to lower cloud droplet number concentration and consequently weaker shortwave cloud cooling. The resulting net top-of-atmosphere radiative response to fuel substitutions ranges from 0.19 to 0.34 W m^{-2}, with the strongest responses over subtropical oceans. Despite similar sulfate reductions, LNG produces the weakest radiative response, whereas blue ammonia produces the strongest, highlighting the influence of co-emitted species and cloud sensitivity beyond sulfur alone.

Keywords: Shipping. Decarbonization. Fuel transition. Earth system modelling.

Introduction

Limiting warming to 2°C during this century will require reducing anthropogenic emissions, particularly carbon dioxide and other greenhouse gases (GHGs), implying a gradual phase out of fossil fuels and the adoption of alternative energy carriers. The feasibility and complexity of this transition vary between sectors. Shipping contributes nearly 3% of global anthropogenic CO_2 emissions, and its comparatively limited near-term mitigation options indicate that its relative emissions share is likely to increase, underscoring its status as a hard-to-abate sector [1–3]. The sector remains heavily dependent on fossil fuels, and although operational and technical efficiency improvements can reduce fuel consumption, most long-term mitigation pathways indicate that substantial emission reductions will

ultimately require a transition toward alternative marine fuels with lower life cycle greenhouse gas intensities [4,5].

Measuring the climate implications of alternative fuels remains challenging, since measures targeting specific pollutants may introduce trade-offs across climate and air quality objectives. The International Maritime Organization (IMO) 2020 sulfur cap provides an opportunity to examine how an abrupt sector-wide emission change affects atmospheric radiation. The reduction in SO_2 emissions lead to a decline in sulfate aerosol formation and its associated cooling influence [6,7]. Satellite observations and aircraft measurements document a post-2020 decline in detectable ship tracks [8–10], while cloud responses beyond visible tracks suggest broader but meteorologically variable changes in clouds microphysics and reflectivity [11,12]. Consequently, the limited representativeness of track-based observations, together with meteorological variability, leaves the global radiative perturbation reliant on model-based estimates. Earlier model estimates of the radiative effect of reduced shipping sulfur emissions span 0.027—0.33 W m^{-2}, reflecting differences in emission perturbations, model frameworks and the treatment of cloud adjustments [13–19].

The uncertainty surrounding the radiative response to sulfur reductions, therefore, points to broader challenge in evaluating marine fuel transitions. For liquefied natural gas, methane slip and upstream emissions may offset the anticipated benefit of lower CO_2 emissions[20,21], and ammonia may influence the nitrogen cycle and lead to N_2O emissions [22–25], a greenhouse gas with a 100-year global warming potential about 273 times higher than CO_2. Other alternatives, including hydrogen, biofuels, and e-fuels, may have varying upstream emissions depending on the primary energy source, while also introducing challenges related to storage, infrastructure, and energy efficiency [26–32].

So far, the literature has investigated the climate impact of alternative marine fuels using life cycle assessment, translating multi-species emissions into climate metrics such as global warming potential (GWP) for 20 and 100 years to reflect near-term versus longer-term climate effects [30,33–36]. These time horizons weigh emissions over different integration periods, although their interpretation depends on the climate metric and temperature goal being considered[37]. While such studies are essential for comparing fuel pathways on a well-to-wake basis, life cycle metrics alone do not fully capture the climate implications of shipping emissions, and do not simulate chemical interactions and aerosol cloud responses that influence radiative forcing for short-lived climate forcers [38–40]. Combining well-to-wake life cycle assessment with atmospheric chemistry and climate modeling can therefore provide a more complete assessment of climate trade-offs among fuels and mitigation strategies[41].

This study asks how the climate impacts of alternative marine fuels change when both well-to-wake emissions and process-based atmospheric responses are considered. This study applies an integrated workflow that links well-to-wake emissions accounting with process-based climate response. Shipping emissions are calculated using the MariTeam model, which provides a bottom-up representation of maritime activity with high spatial and temporal resolution [41,42]. These emissions are then used as input to the Norwegian Earth System Model, NorESM2 [43], to simulate the climate-relevant response across well-mixed greenhouse gases (CO_2, CH_4, N_2O) and co-emitted short-lived species (SO_2, SO_4, CO, BC, PM2.5). The next section details the scenario design, emissions calculation, and aggregation to model-ready inputs, and the NorESM2 experiment configuration used to quantify effective radiative forcing and temperature responses attributable to each scenario. The novelty lies in linking a high-resolution, well-to-wake shipping emissions inventory with an Earth system model whilst comparing a range of alternative fuel options. This integrated framework captures climate trade-offs that are missed when fuel pathways are assessed using life cycle metrics alone, allowing the contributions of greenhouse gases and short-lived co-emitted species to be quantified within a common modeling system.

Methods

MariTeam

The MariTeam model (Maritime Transport Environmental Assessment Model) is a bottom-up framework for ship emission quantification that integrates ship positional data with technical vessel specifications and ship resistance models to estimate the energy demand and associated emissions from the maritime sector[41,42]. The model employs Automatic Identification System (AIS) data to determine ship positions (latitude and longitude) and speed over time, as recorded by terrestrial receivers and the NorSat-1 and NorSat-2 satellites. The dataset comprises approximately 15 billion AIS messages collected between 2019 and 2025, representing 88,000 vessels. The routes were completed for shorter time intervals (0.1° latitude-longitude resolution) using the A* path-search algorithm in combination with Dijkstra's algorithm[41,44]. In total, 37% of AIS messages used were generated by the algorithm, in particular for heavily trafficked regions. To account for weather conditions, each AIS observation is linked with wind and sea state parameters from the ERA-Interim reanalysis produced by the European Centre for Medium-Range Weather Forecasts (ECMWF). Technical ship characteristics, including hull and engine dimensions required for ship resistance modelling, are obtained from the Sea-web Ships database, while any missing parameters are estimated following the methodology of Kim et al. (2022)[45]. Ship resistance is subsequently evaluated using a meta-model developed by Kim et al. (2023)[42], which integrates calm-water resistance with additional wind and wave resistance components.

The emissions calculated in the model cover the main greenhouse gases (CO_2, CH_4, N_2O) and other pollutants (NO_x, SO_2, SO_4, CO, OC, EC, BC). The baseline experiment calculates the emissions based on the 2019 fuel mix, i.e. before any COVID-19 adjustments to shipping traffic and emissions[46] and before the IMO 2020 sulfur emissions cap[47]. corresponding to an approximate share of 70% heavy-fuel oil (HFO), 29% Marine gas oil (MGO), and 1% Liquefied natural gas (LNG). The MariTeam model is also designed to run the shipping fleet with different fuels. In this study, we will assess emission outcomes from running the entire fleet on the same fuel for the following cases: Conventional heavy-fuel oil (HFO), Marine gas oil (MGO), Very-low sulfur fuel oil (VLSFO), Liquefied natural gas for high-pressure engines (LNGhp), Blue ammonia (blueNH3). Blue ammonia is made by steam methane reforming into hydrogen with most of the CO_2 captured. The hydrogen is then combined with nitrogen from the air in the Haber–Bosch process to make ammonia. We present a summary of emissions data derived from the MariTeam model in Figure 1.

Using the MariTeam model, four marine fuel and propulsion scenarios were simulated:

1. Current fuel mix: This baseline scenario represents the current fleet operating on conventional marine fuels. Heavy fuel oil (HFO) is used outside emission control areas (ECAs), while marine gas oil (MGO) is used within ECAs and by 4-stroke engines, and LNG is used mostly for gas tankers.
2. Very-Low-sulfur fuel: This scenario reflects compliance with the IMO global sulfur cap implemented in 2020, limiting fuel sulfur content to 0.5% mass by mass. HFO is replaced by very-low-sulfur distillate fuels across the global fleet.
3. LNG switch: This scenario assumes a switch towards high-pressure dual-fuel engines operating primarily on liquefied natural gas (LNG), with MGO used as pilot fuel. LNG is treated as a transitional fuel that reduces particulate matter and sulfur emissions relative to conventional fuels.

4. Ammonia Fuel: This scenario represents a switch to ammonia-based propulsion in dual-fuel marine engines. Ammonia is assumed to be used as primary fuel, with hydrogen as pilot fuel. The scenario assumes that engines currently designed for LNG operation could be adapted to ammonia with limited retrofitting.

We adopt ammonia as a potential low-emission maritime fuel due to its carbon-free combustion and relatively favorable storage properties compared to hydrogen. Ammonia liquefies at approximately −33°C, whereas hydrogen requires cryogenic storage at approximately −253°C, posing greater challenges for onboard storage and distribution infrastructure[48]. Fuel-cell and battery-electric propulsion systems are excluded from this study, which focuses on combustion-based propulsion. These alternatives require separate assessments of onboard energy storage, system integration and voyage requirements[49,50], which is beyond the scope of this study.

NorESM

Simulations for this study were carried out using the second generation of the Norwegian Earth System Model (NorESM2), a fully coupled Earth system model that contributed to the sixth phase of the Coupled Model Intercomparison Project (CMIP6) [43]. The atmospheric component of NorESM2 is CAM-Oslo, which builds upon the Community Atmosphere Model version 6 (CAM6) (Table 1), while replacing the default aerosol scheme with an interactive aerosol module. This feature of CAM-Oslo provides a highly detailed representation of aerosol-radiation and aerosol-cloud interactions. This high-fidelity representation of aerosol indirect effects is a strong driver of the model's transient climate response (TCR) and equilibrium climate sensitivity (ECS)[43], making it particularly robust for studies involving anthropogenic emission perturbations and atmospheric forcing.

Experimental design:

We have conducted atmosphere-only experiments in NorESM, using MariTeam emissions for alternative fuels to define the perturbations used. The atmosphere-only experiments are a type of climate simulation carried out under the Atmospheric Model Intercomparison Project (AMIP), in which atmospheric models are run using prescribed sea surface temperatures and sea ice distributions, allowing the isolation and study of the atmospheric response to these surface boundary conditions without the added complexity of coupled ocean-atmosphere interactions. Unlike transient climate simulations, which model the continuous evolution of climate over time, we use a time-slice experiment that focuses on a single period cycle simulated to represent year 2019. The simulation duration was about 24 years, where the first 4 years correspond to a spin-up phase (transient phase of the simulation) followed by a steady-state.

Table 1 NorESM model set-up

Model Property	**Value**
Model version	NorESM2.0.6
Horizontal resolution	0.9x1.25 degrees
Atmospheric version	CAM6-Nor
Aerosol version	OsloAero6
Vertical resolution atmosphere	30 levels
Ozone and NOx concentrations	CESM2-WACCM
SST	Fixed values prescribed from 2019
Sea ice component	Prescribed 2019
Vegetation	Prescribed CLM5.0%BGC

All simulations are conducted as time-slice experiments centred on 2019, consistent with the shipping emission inventory generated with the MariTeam model. Large-scale background climate forcing follows the SSP2-4.5 scenario from the Coupled Model Intercomparison Project Phase 6 (CMIP6) for the year 2019. In practice, we adopt forcing datasets from a previous NorESM experiment conducted under SSP2-4.5 conditions, which provide the prescribed greenhouse gas concentrations, oxidant fields, and emissions of short-lived species.

Greenhouse gas concentrations are prescribed as globally uniform surface mixing ratios (ppmv) and are used in the model radiative transfer calculations. Vertical distributions are derived from latitudinally varying, species-specific profiles that determine concentrations at different altitudes.

Monthly three-dimensional oxidant fields are prescribed to represent the background atmospheric chemical environment. These include OH, O_3, NO_3, and H_2O_2, which control the oxidation pathways of key species such as dimethyl sulfide (DMS), sulfur dioxide (SO_2), isoprene, and monoterpenes. Oxidant concentrations influence the formation of secondary aerosols, particularly sulfate and secondary organic aerosols (SOA). Emissions of short-lived species are prescribed with monthly temporal resolution and include two- and three-dimensional spatial distributions of anthropogenic and natural sources.

We performed six NorESM simulations to assess the climate effects of alternative shipping fuels (Table 2). A control simulation excluding shipping emissions (NoShip) provided the reference for five experiments representing the 2019 fuel mix (Fmix), its tank-to-wake emissions only ($Fmix_{TTW}$), very-low-sulfur fuel oil (VLSFO), liquefied natural gas used in high-pressure engines (LNGhp), and blue ammonia (blueNH3).

Table 2 List of NorESM experiments

Experiment	Short names
Control without shipping emissions	***NoShip***
2019 fuel mix WTW	***Fmix***
2019 fuel mix TTW	***$Fmix_{TTW}$***
Very low Sulfur fuel oil	***VLSFO***
LNG	***LNGhp***
Blue Ammonia	***blueNH3***

Results

Emissions from MariTeam

Annual global well-to-wake (WTW) emissions, comprising tank-to-wake (TTW) and well-to-tank (WTT) contributions, varied markedly among fuel pathways (Figure 1). TTW emissions dominated CO_2 emissions for carbon-based fuels, whereas ammonia-related CO_2 emissions arose from WTT processes. TTW contributions dominated organic carbon emissions across all pathways and CH_4 emissions for all except ammonia, while both stages contributed substantially to CH_4 emissions from LNG. Ammonia yielded the lowest CO_2 emissions but the highest N_2O emissions, predominantly from TTW processes. LNG and ammonia substantially reduced SO_2, and black carbon emissions as expected, highlighting trade-offs between lower emissions of these pollutants and higher emissions of non-CO_2 greenhouse gases.

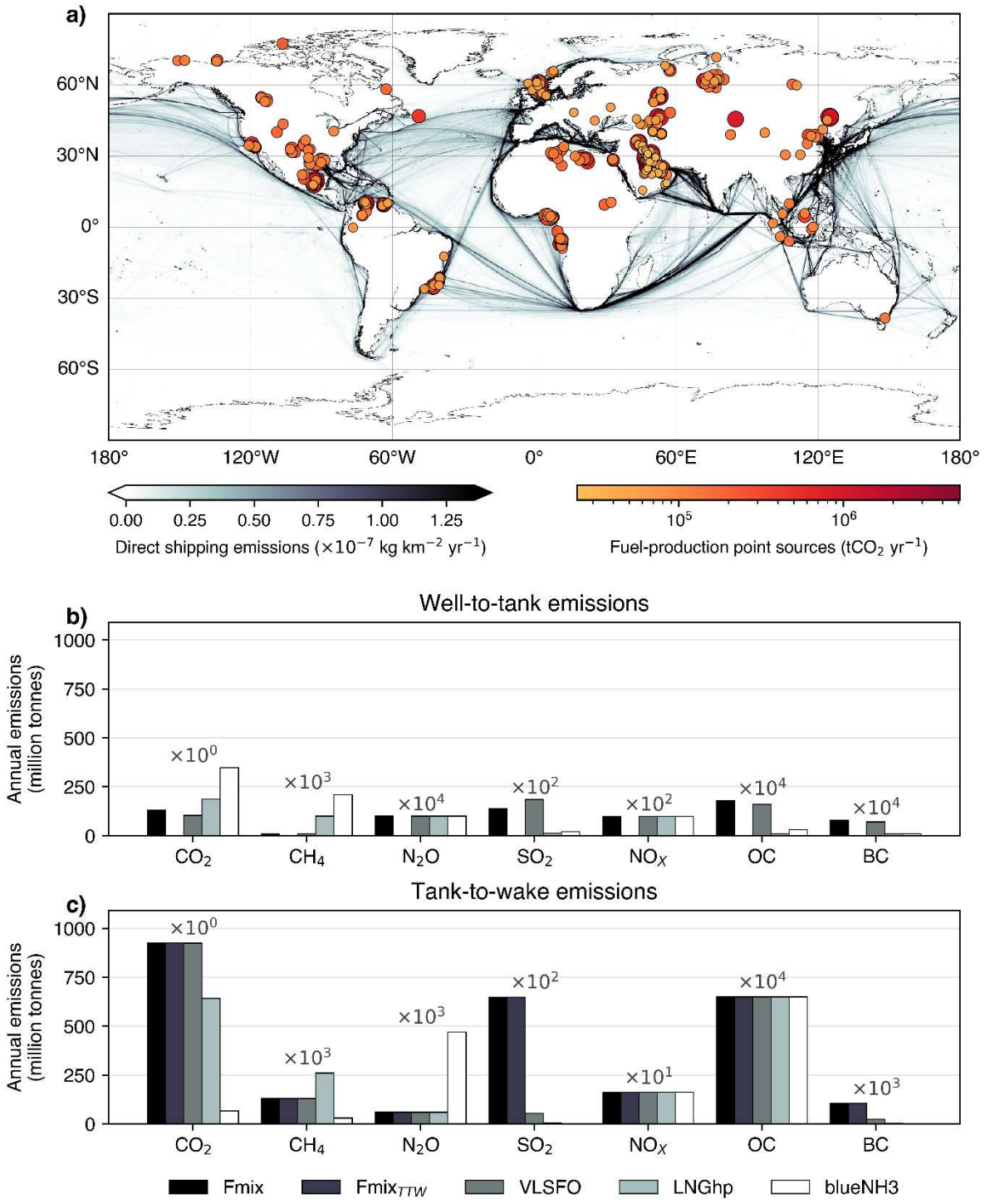


Figure 1 Annual global marine fuels emissions from MariTeam, separated into well-to-tank (WTT) and tank-to-wake (TTW) components. The map shows CO_2 emissions from fuel production ($tCO_2\ yr^{-1}$) on brown scale and shipping direct CO_2 emission on black scale. Bar charts show emissions (million tonnes) of CO_2, CH_4, N_2O, SO_2, NO_x, organic carbon (OC), and black carbon (BC) for five fuel types: heavy fuel oil (HFO), marine fuel mix (Fmix), very-low-sulfur fuel oil (VLSFO), high-pressure liquefied natural gas (LNGhp), and ammonia (blueNH3). Note different scales on bars (10^x).

Aerosol effects

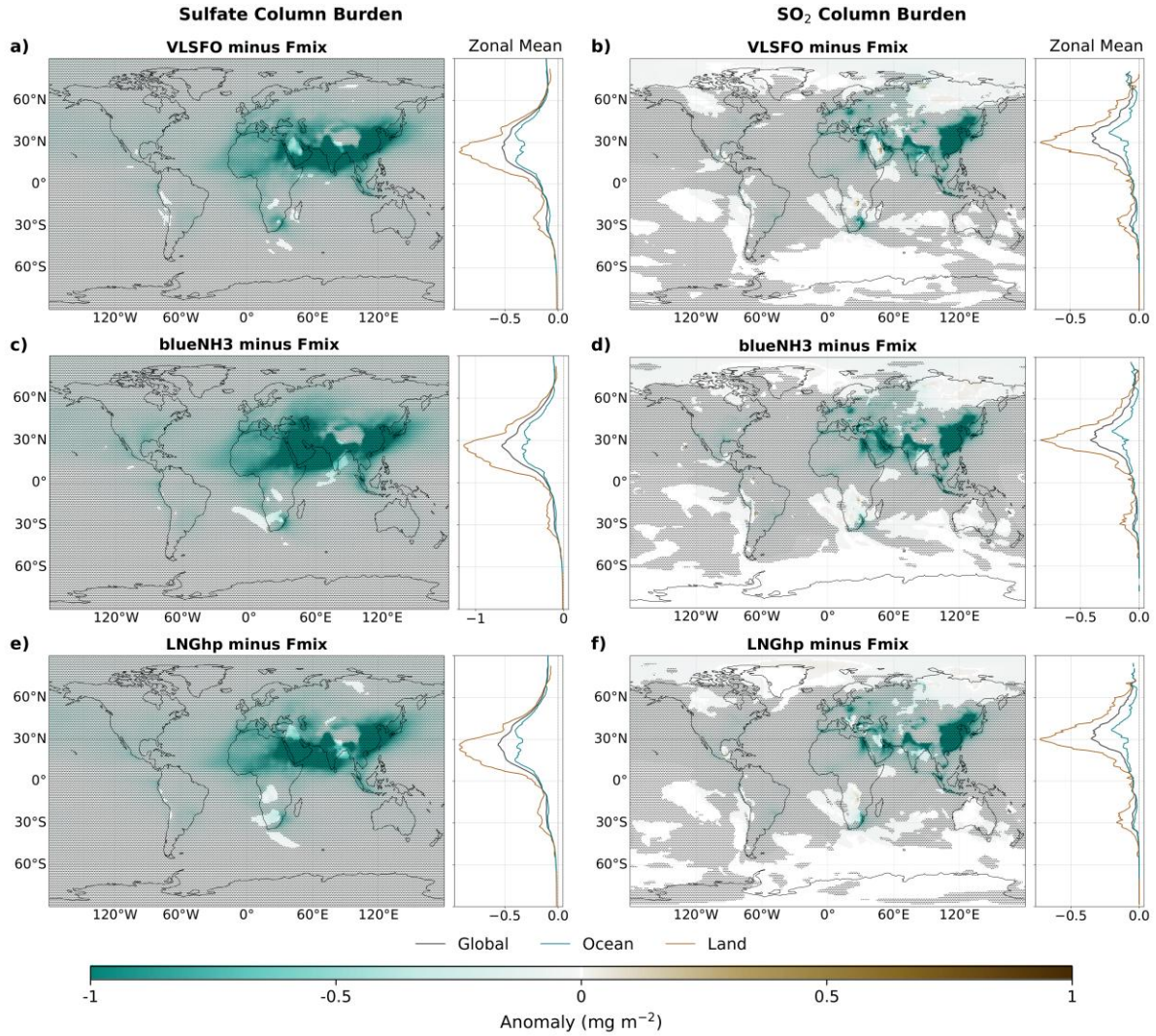


Figure 2 Changes in SO_4 and SO_2 burden in a), b) VLSFO, c), d) blueNH3 and e), f) LNGhp cases relative to Fmix. Map shading and zonal profiles show anomalies in mg m^{-2}. Black stippling marks grid cells with $p < 0.05$ in a Student's t-test. Side panels show zonal means over significant grid cells within the global, ocean and land domains represented by black, blue, and brown lines, respectively.

All alternative maritime fuel cases reduced the atmospheric column burden of SO_2 and SO_4 relative to Fmix baseline with broadly similar spatial patterns (Figure 2). Near-surface SO_2 concentration (Supplementary Figure 1) decreases by about 23-26%; the corresponding SO_2 column burden by about 13-14%, and SO_4 column burden by about 12-14% across alternative fuel cases. The largest reductions compared to 2019 fuel mix occur along Northern Hemisphere mid-latitudes shipping corridors and adjacent downwind continental areas (Fig. 2). Means over land domain are more negative than ocean means for both SO_2 and SO_4, demonstrating that the sulfur column burden perturbations extend beyond the ocean.

The conventional shipping perturbation reverses the sign of sulfur response. In Fmix minus NoShip, global mean column burden of SO_2 and sulfate increase, whereas all alternative fuel cases reduce both burdens relative to Fmix, with the largest global mean reductions in blueNH3.

Carbonaceous aerosol responses differ substantially among fuel pathways (Figure 3). VLSFO shows relatively small changes in carbonaceous aerosol burdens relative to Fmix: global black carbon (BC)

burden increases by about 0.5%, and organic carbon (OC) burden increases by about 0.2%. blueNH3 reduces BC and OC column burden by about 76% and 12% respectively, as well as reducing the bottom-layer BC concentration (Supplementary Figure 2) by about 80%. LNGhp scenario reduces global BC column burden by about 53% and surface BC by ~56%, with similar percentage reductions over ocean and land domains. However, its global mean OC burden change is relatively small (- 0.03%). Thus, VLSFO primarily reduces the sulfur aerosol pathway, LNGhp reduces sulfur and black carbon, and blueNH3 gives the clearest combined reduction in sulfur and carbonaceous burdens.

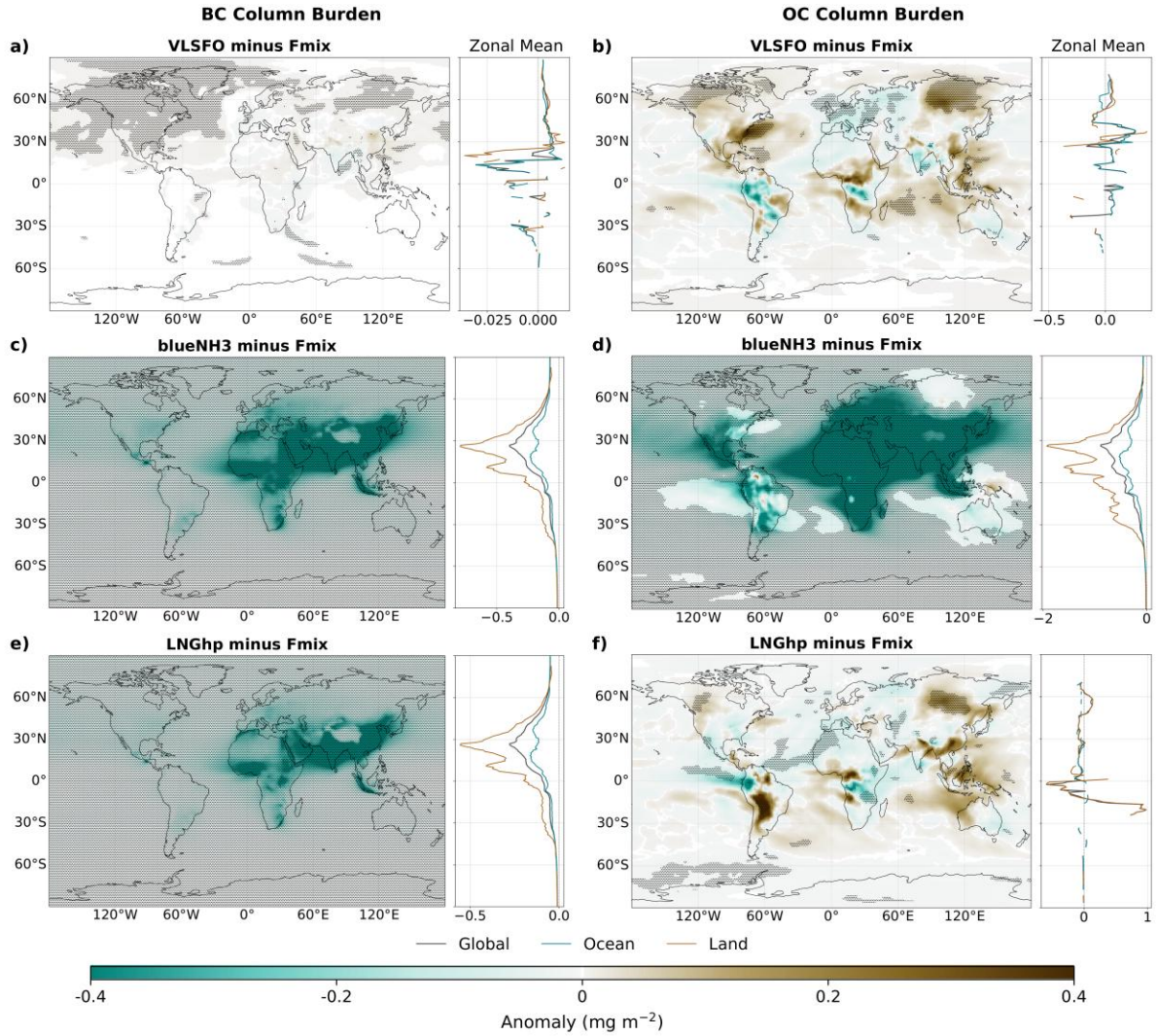


Figure 3 Changes in black carbon and organic carbon column burdens in a), b) VLSFO, c), d) blueNH3 and e), f) LNGhp cases relative to Fmix. Map shading and zonal profiles show anomalies in mg m^{-2}. Black stippling and zonal mean side panels are defined as in Fig. 2.

Cloud microphysical response

The perturbation of the aerosol population can modify cloud microphysical properties, primarily through a reduction in available cloud condensation nuclei, if shipping aerosol emissions are reduced. This can initiate a Twomey effect[51,52], characterized by a decrease in cloud droplet number concentration and a compensatory increase in droplet effective radius.

Vertically integrated cloud droplet number concentration (CDNC) decreases in all alternative fuel cases relative to Fmix. Mean global reductions are approximately 2.7%, 3.3%, and 5.3% in LNGhp, VLSFO, and blueNH3 respectively (Fig. 4). The largest decrease occurs in blueNH3, consistent with its

strongest sulfate and carbonaceous aerosol reduction. Statistically significant vertically integrated CDNC anomalies cover a much smaller fraction of the global domain than sulfate anomalies. Within significant grid cells, mean reductions are 6.7%, 8.2% and 10.8% in LNGhp, VLSFO, and blueNH3, respectively.

Changes in cloud droplet effective radius were small, with increases over ocean and decreases over land in all three cases (Supplementary Figure 3). The marine response is qualitatively consistent with fewer, larger droplets following reduced aerosol availability. However, column-integrated droplet number and effective radius alone do not isolate the Twomey effect; changes in cloud liquid water and cloud extent also need be considered.

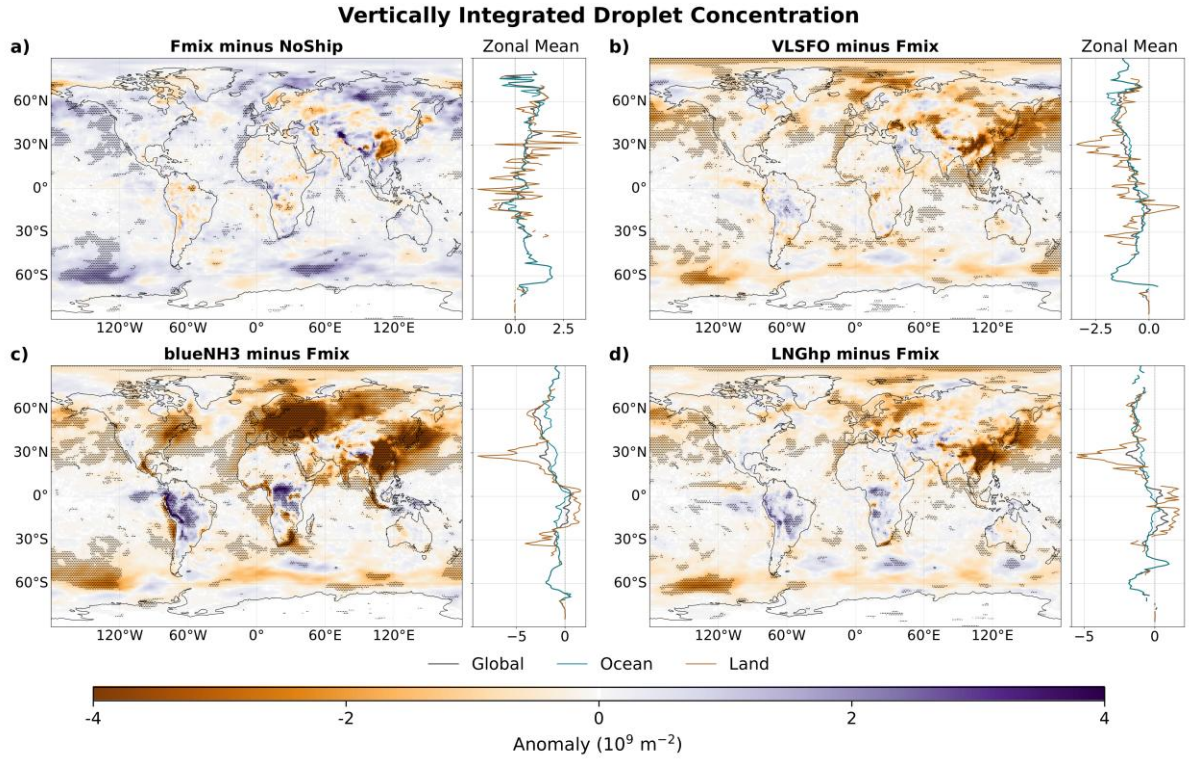


Figure 4 Changes in vertically integrated cloud droplet number concentration for a) Fmix relative to NoShip, and b) VLSFO, c) blueNH3 and d) LNGhp relative to Fmix. Map shading and zonal profiles show anomalies in 10^9 m^{-2}. Black stippling and zonal mean side panels are defined as in Fig. 2.

Cloud radiative cooling and effective radiative forcing

The global mean shortwave cloud radiative response changes sign between the conventional and alternative fuel perturbations. The mean global shortwave cloud forcing (SWCF) anomaly is negative in Fmix minus NoShip, indicating enhanced shortwave cloud cooling associated with conventional shipping emissions. Relative to Fmix, all alternative fuel cases produce positive SWCF anomalies: +0.35 W m^{-2}, +0.28 W m^{-2}, and +0.37 W m^{-2} in VLSFO, LNGhp and blueNH3 respectively (Fig. 5). These positive anomalies indicate weaker shortwave cloud cooling.

The mean global TOA flux differences provide an estimate of effective radiative forcing for the prescribed perturbations, including rapid adjustments, with sea surface temperature response suppressed. Global mean values of net top-of-atmosphere (TOA) radiative flux anomalies relative to Fmix are positive in all alternative fuel cases: +0.31 W m^{-2} in VLSFO, +0.19 W m^{-2} in LNGhp, and +0.34 W m^{-2} in blueNH3 (Fig. 6), consistent with the weakened shortwave cloud cooling. The positive global means concealing substantial regional heterogeneity, with positive anomalies across broad

areas of the subtropical oceans and negative anomalies in parts of the Southern Ocean. The net TOA anomalies were smaller than the corresponding shortwave cloud anomalies by approximately 0.04, 0.09 and 0.03 W m^{-2} in VLSFO, LNGhp, and blueNH3, respectively. This difference indicates a net negative contribution from the combined clear-sky shortwave and all-sky longwave changes, partially offsetting the positive anomaly associated with weakened shortwave cloud cooling. The mean anomaly of net TOA radiative flux over ocean is positive in all three cases, whereas land - only means are weakly negative for LNGhp and blueNH3, showing that the radiative response can differ in sign between land and ocean despite the positive global mean.

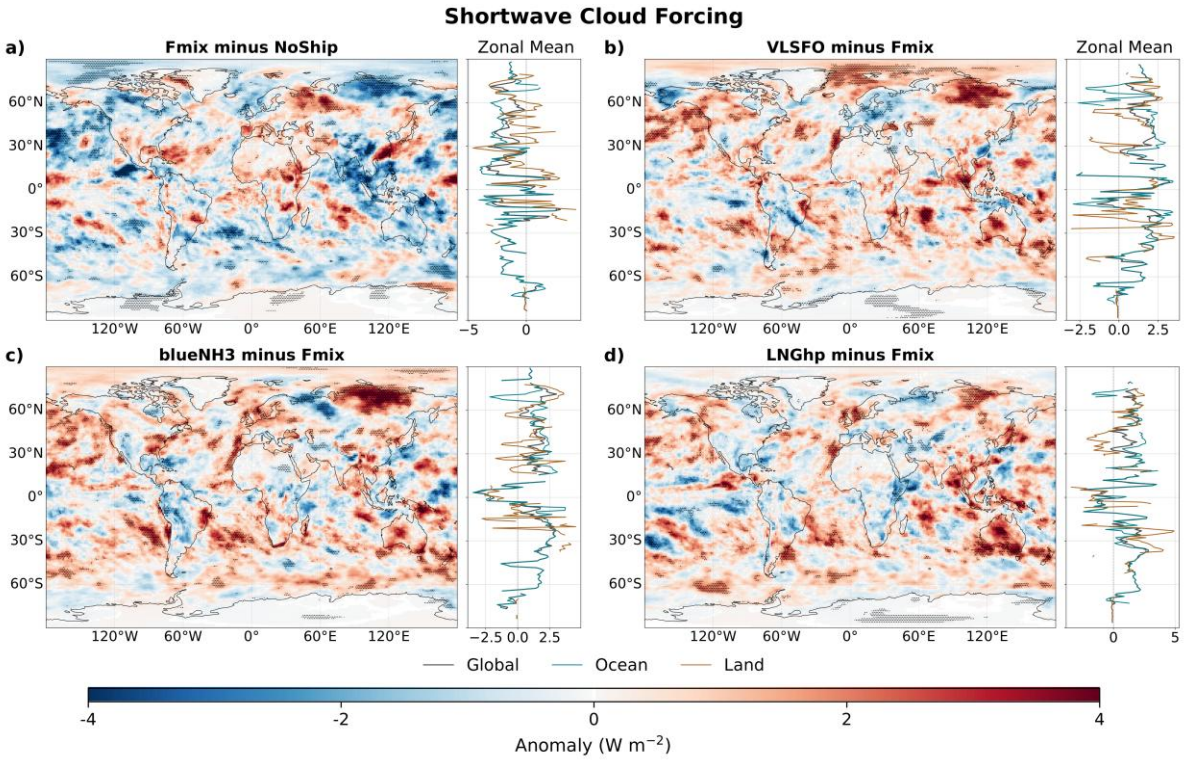


Figure 5 Changes in shortwave cloud forcing for a) Fmix relative to NoShip, and b) VLSFO, c) blueNH3, and d) LNGhp relative to Fmix. Map shading and zonal profiles show anomalies in W m^{-2}. Black stippling and zonal mean side panels are defined as in Fig. 2.

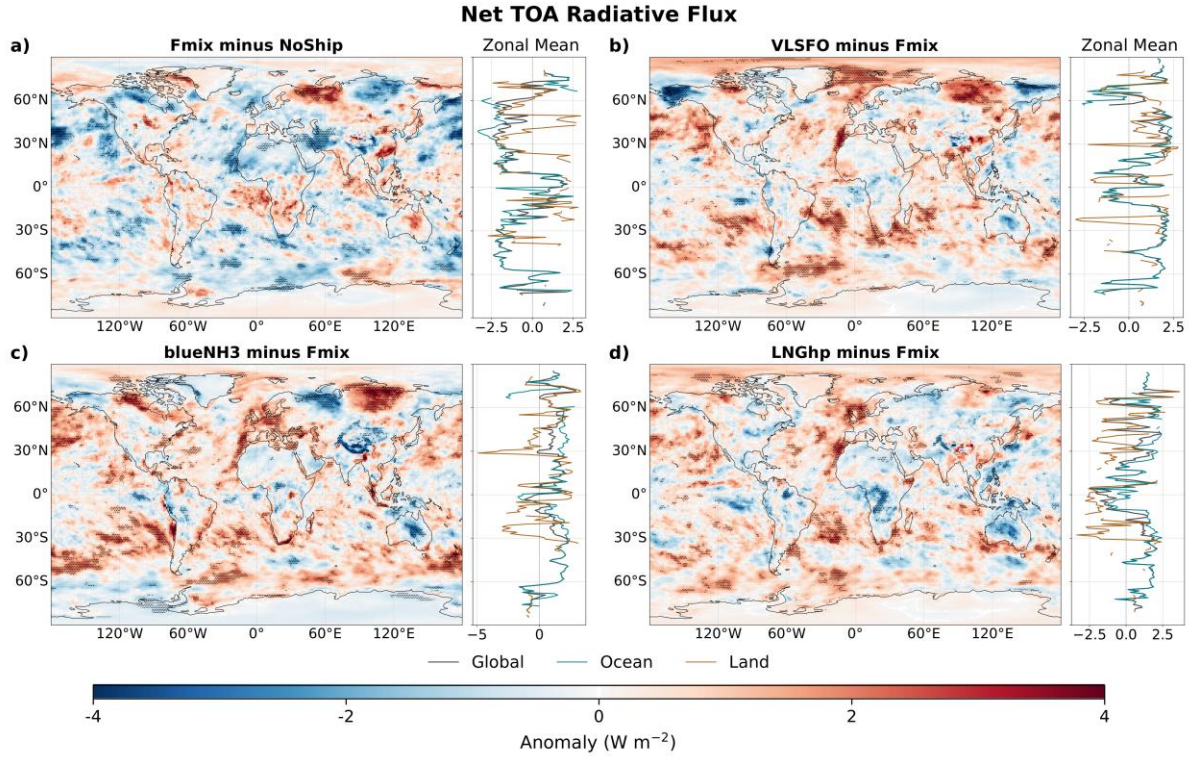


Figure 6 Changes in net radiative flux at the top of atmosphere for a) Fmix relative to NoShip, and b) VLSFO, c) blueNH3, and d) LNGhp relative to Fmix. Map shading and zonal profiles show anomalies in W m^{-2}. Black stippling and zonal mean side panels are defined as in Fig. 2.

Precipitation responses

Global mean convective precipitation increases slightly in all three alternative fuel cases relative to Fmix. The response (Fig. 7) shows alternating positive and negative anomalies across the Intertropical Convergence Zone, the Maritime Continent, tropical Africa, Central America, and the tropical Pacific, and Indian oceans. LNGhp and blueNH3 show similar tropical patterns as VLSFO, with larger positive oceanic zonal-mean anomalies in the Northern Hemisphere tropics and subtropics. These zonal averages are restricted to statistically significant grid cells, with spatial masks that may differ among experiments. The convective response therefore shows substantial regional contrasts despite the small positive global mean.

Total precipitation exhibits additional extratropical anomalies beyond the predominantly tropical convective response (Figure 8). In VLSFO, global total precipitation change is slightly negative (-0.001 mm day^{-1}) despite a small convective increase implying an offsetting decrease in the large-scale precipitation component. LNGhp and blueNH3 show small positive global total precipitation changes, but their maps show opposing local anomalies rather than a uniform wetting response. Together, these results show spatially heterogeneous precipitation responses with small global mean changes. The fixed-SST experiments capture the fast hydrological response to the prescribed shipping-emission perturbations, with ocean-temperature-mediated responses excluded.

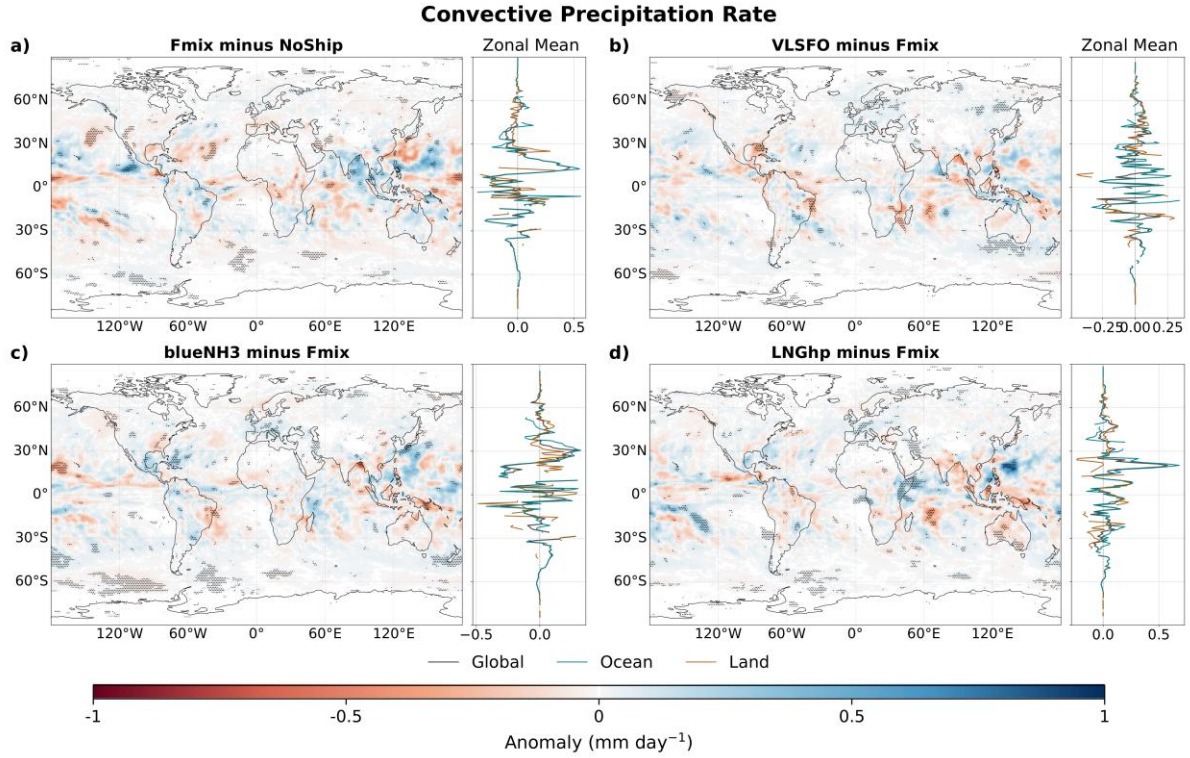


Figure 7 Changes in convective precipitation rate, including liquid and ice, for a) Fmix relative to NoShip, and b) VLSFO, c) blueNH3 and d) LNGhp relative to Fmix. Map shading and zonal profiles show anomalies in mm day^{-1}. Black stippling and zonal mean side panels are defined as in Fig. 2.

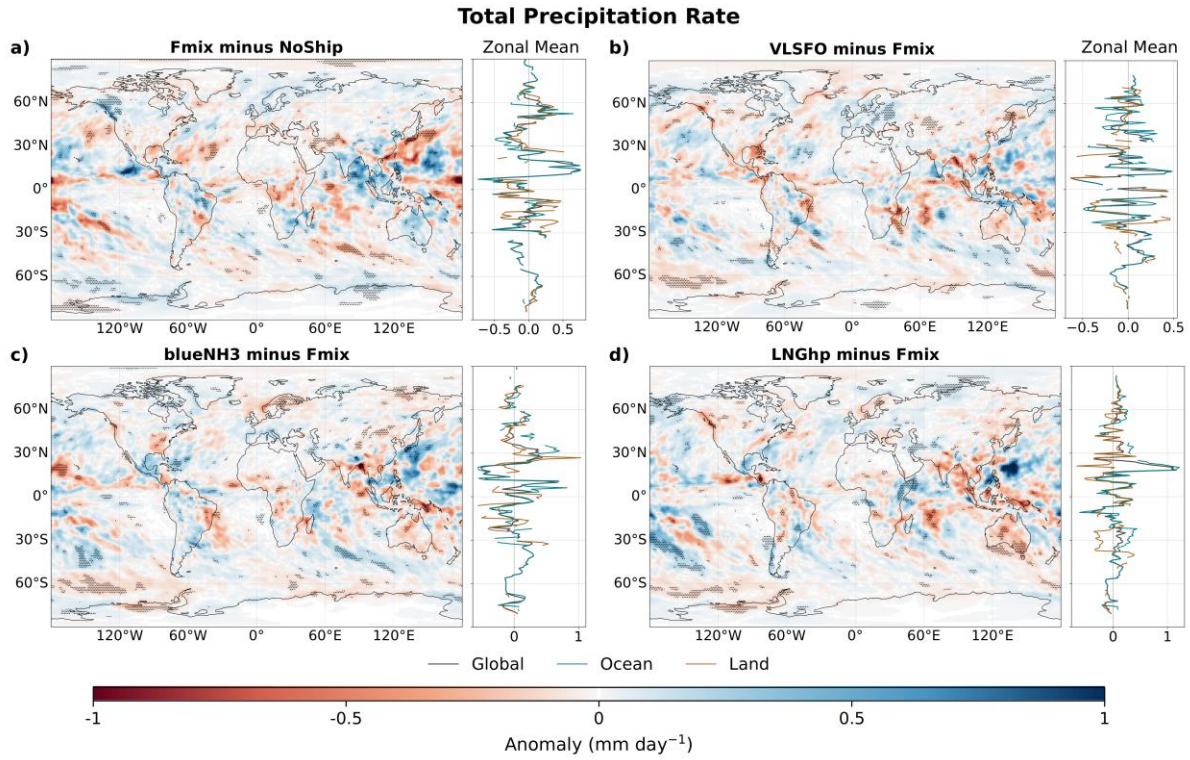


Figure 8 Changes in total precipitation rate, including liquid and ice, for a) Fmix relative to NoShip, and b) VLSFO, c) blueNH3 and d) LNGhp relative to Fmix. Map shading and zonal profiles show anomalies in mm day^{-1}. Black stippling and zonal mean side panels are defined as in Fig. 2.

Discussion

Alternative marine fuels reduce sulfate burdens and weaken shortwave cloud cooling relative to the conventional fuel mix. This is consistent with previous assessments of reduced aerosol-induced coopling following low-sulfur shipping regulations [53], and the positive forcing diagnosed in coordinated fixed-SST experiments after a shipping sulfur cap[7]. In the AMIP experiments performed here, fuel substitution modifies multiple aerosol and precursor emissions simultaneously. Despite broadly comparable reductions in sulfur burden reductions, the experiments lead to different cloud droplet numbers and top-of-atmosphere radiative responses across alternative fuel cases.

The ordering of the mean responses differs among diagnostics. Sulfate burden reductions are largest for blueNH3, followed by LNGhp, and VLSFO – following their corresponding reductions in sulfur content of the fuels, whereas cloud droplet number reduction, positive shortwave cloud radiative anomalies, and net TOA radiative anomalies follow the order blueNH3, VLSFO, and LNGhp. This difference in ordering suggests that sulfur-burden reductions alone may not explain cloud and radiative responses.

The cloud response provides a plausible link between aerosol changes and the radiative signal, although the underlying processes are not fully isolated. The spatially heterogeneous cloud-droplet and radiative anomalies are consistent with responses that depend on background aerosol conditions, cloud regime, and meteorological state. Such dependence is consistent with previous studies [11,51,54–56]. The simulations therefore show a coherent aerosol cloud radiation sequence, but not a fully attributed mechanism for fuel dependent differences.

The positive net TOA response is consistent with weakened shortwave cloud cooling while also integrating other shortwave and longwave contributions. The simulated anomalies are positive for all alternative fuels, spanning +0.19 to +0.34 W m^{-2} relative to Fmix. Under prescribed SST and sea ice, the TOA response includes the instantaneous radiative perturbation and rapid adjustments of the atmosphere, clouds and land surface, while suppressing responses mediated by changes on ocean temperature [57,58]. Small global mean precipitation changes coexist with substantial regional contrasts, emphasizing the need to assess hydrological responses and their uncertainty at both scales for alternative fuels.

These results indicate that sulfur content alone is insufficient to characterize the climate outcomes of alternative marine fuels. These fixed SST simulations constrain the radiative response to the prescribed shipping emission changes but cannot, on their own, establish a holistic assessment of climate and sustainability implications of transitioning to alternative marine fuels. Such assessments would also depend on full life cycle GHG emissions and the time horizon over which climate impacts are evaluated, as well as on broader environmental, economic and social considerations. Within the experimental scope tested here, alternative marine fuel adoption produces a positive net TOA radiative anomaly relative to Fmix, with a magnitude that varies among fuel pathways.

Acknowledgments

This work was supported by Research Council of Norway (RCN) projects Bio4-7Seas (no. 302276), CLIMMS (no. 294771), SFI Smart Maritime (no. 237917), FME MarTrans (no. 350371), and NorESM4CMIP7 (no. 352204), as well as Sigma2 — the Norwegian National Infrastructure for High-Performance Computing and Data Storage resources under projects NN9576K, NS9576K, and NS9083K.

Data availability: data is available upon request and in accordance with the journal's policies and procedures.

Competing interests: The authors declare no competing interests.

References

1. Deng, S. & Mi, Z. A review on carbon emissions of global shipping. *Mar Dev* **1**, 4 (2023).
2. Faber, J. *et al.* Fourth imo ghg study. *London, UK* (2020).
3. Müller-Casseres, E. *et al.* International shipping in a world below 2 °C. *Nat. Clim. Chang.* **14**, 600–607 (2024).
4. Bouman, E. A., Lindstad, E., Rialland, A. I. & Strømman, A. H. State-of-the-art technologies, measures, and potential for reducing GHG emissions from shipping – A review. *Transportation Research Part D: Transport and Environment* **52**, 408–421 (2017).
5. Gilbert, P. *et al.* Assessment of full life-cycle air emissions of alternative shipping fuels. *Journal of Cleaner Production* **172**, 855–866 (2018).
6. Sofiev, M. *et al.* Cleaner fuels for ships provide public health benefits with climate tradeoffs. *Nat Commun* **9**, 406 (2018).
7. Skeie, R. B., Byrom, R., Hodnebrog, Ø., Jouan, C. & Myhre, G. Multi-model effective radiative forcing of the 2020 sulfur cap for shipping.
8. Watson-Parris, D. *et al.* Shipping regulations lead to large reduction in cloud perturbations. *Proc. Natl. Acad. Sci. U.S.A.* **119**, e2206885119 (2022).
9. Yuan, T. *et al.* Global reduction in ship-tracks from sulfur regulations for shipping fuel. *Sci. Adv.* **8**, eabn7988 (2022).
10. Lee, J. D. *et al.* SO_2 and NO_x emissions from ships in North-East Atlantic waters: *in situ* measurements and comparison with an emission model. *Environ. Sci.: Atmos.* **5**, 1282–1296 (2025).
11. Manshausen, P., Watson-Parris, D., Christensen, M. W., Jalkanen, J.-P. & Stier, P. Invisible ship tracks show large cloud sensitivity to aerosol. *Nature* **610**, 101–106 (2022).

12. Diamond, M. S. Detection of large-scale cloud microphysical changes within a major shipping corridor after implementation of the International Maritime Organization 2020 fuel sulfur regulations. *Atmos. Chem. Phys.* **23**, 8259–8269 (2023).
13. Bilsback, K. R. *et al.* Beyond SO_x reductions from shipping: assessing the impact of NO_x and carbonaceous-particle controls on human health and climate. *Environ. Res. Lett.* **15**, 124046 (2020).
14. Gettelman, A. *et al.* Has Reducing Ship Emissions Brought Forward Global Warming? *Geophysical Research Letters* **51**, e2024GL109077 (2024).
15. Jin, Q., Grandey, B. S., Rothenberg, D., Avramov, A. & Wang, C. Impacts on cloud radiative effects induced by coexisting aerosols converted from international shipping and maritime DMS emissions. *Atmos. Chem. Phys.* **18**, 16793–16808 (2018).
16. Jordan, G. & Henry, M. IMO2020 Regulations Accelerate Global Warming by up to 3 Years in UKESM1. *Earth's Future* **12**, e2024EF005011 (2024).
17. Partanen, A. I. *et al.* Climate and air quality trade-offs in altering ship fuel sulfur content. *Atmos. Chem. Phys.* **13**, 12059–12071 (2013).
18. Yoshioka, M., Grosvenor, D. P., Booth, B. B. B., Morice, C. P. & Carslaw, K. S. Warming effects of reduced sulfur emissions from shipping. *Atmos. Chem. Phys.* **24**, 13681–13692 (2024).
19. Quaglia, I. & Visioni, D. Modeling 2020 regulatory changes in international shipping emissions helps explain anomalous 2023 warming. *Earth System Dynamics* **15**, 1527–1541 (2024).
20. Balcombe, P. *et al.* How can LNG-fuelled ships meet decarbonisation targets? An environmental and economic analysis. *Energy* **227**, 120462 (2021).
21. Pavlenko, N., Comer, B., Zhou, Y., Clark, N. And Rutherford, D. The climate implications of using LNG as a marine fuel. (2020).
22. Chalaris, I., Jeong, B. & Jang, H. Application of parametric trend life cycle assessment for investigating the carbon footprint of ammonia as marine fuel. *The International Journal of Life Cycle Assessment* **27**, 1145–1163 (2022).

23. Wolfram, P., Kyle, P., Zhang, X., Gkantonas, S. & Smith, S. Using ammonia as a shipping fuel could disturb the nitrogen cycle. *Nat Energy* **7**, 1112–1114 (2022).
24. Wong, A. Y. H. *et al.* Climate and air quality impact of using ammonia as an alternative shipping fuel. *Environ. Res. Lett.* **19**, 084002 (2024).
25. Esquivel-Elizondo, S., Walkowiak, B., Sartzetakis, S. S. & Buma, B. Climate Impact of Direct and Indirect N2O Emissions from the Ammonia Marine Fuel Value Chain. *Environ. Sci. Technol.* **59**, 9037–9048 (2025).
26. Douglas, C. M. *et al.* Techno-economic analysis and life-cycle assessment of methanol synthesis plants using renewable hydrogen and carbon dioxide feedstocks. *Energy Conversion and Management* **347**, 120374 (2026).
27. Esfandiari, H., Muri, H. & Kramel, D. Biomethanol as a Marine Fuel Within Land Use Sustainability Boundaries. *Clean Technol.* **7**, 101 (2025).
28. Wang, Y., Xiao, X. & Ji, Y. A Review of LCA Studies on Marine Alternative Fuels: Fuels, Methodology, Case Studies, and Recommendations. *Journal of Marine Science and Engineering* **13**, 196 (2025).
29. Kanchiralla, F. M., Brynolf, S. & Mjelde, A. Role of biofuels, electro-fuels, and blue fuels for shipping: environmental and economic life cycle considerations. *Energy Environ. Sci.* **17**, 6393–6418 (2024).
30. Roux, M., Lodato, C., Laurent, A. & Astrup, T. F. A review of life cycle assessment studies of maritime fuels: Critical insights, gaps, and recommendations. *Sustainable Production and Consumption* **50**, 69–86 (2024).
31. IRENA. *Innovation Landscape for Smart Electrification: Decarbonising End-Use Sectors with Renewable Power*. https://www.irena.org/-/media/Files/IRENA/Agency/Publication/2023/Jun/IRENA_Innovation_landscape_smart_electrification_2023.pdf (2023).

32. McKinlay, C. J., Turnock, S. R. & Hudson, D. A. Route to zero emission shipping: Hydrogen, ammonia or methanol? *International Journal of Hydrogen Energy* **46**, 28282–28297 (2021).
33. Ji, C. & El-Halwagi, M. M. A data-driven study of IMO compliant fuel emissions with consideration of black carbon aerosols. *Ocean Engineering* **218**, 108241 (2020).
34. Levasseur, A. *et al.* Enhancing life cycle impact assessment from climate science: Review of recent findings and recommendations for application to LCA. *Ecological Indicators* **71**, 163–174 (2016).
35. Peng, W. *et al.* Comprehensive analysis of the air quality impacts of switching a marine vessel from diesel fuel to natural gas. *Environmental Pollution* **266**, 115404 (2020).
36. Rezaei, S., Hormaza Mejia, A., Wu, Y., Reed, J. & Brouwer, J. Global warming impacts of the transition from fossil fuel conversion and infrastructure to hydrogen. *Applied Energy* **397**, 126363 (2025).
37. Abernethy, S. & Jackson, R. B. Global temperature goals should determine the time horizons for greenhouse gas emission metrics. *Environ. Res. Lett.* **17**, 024019 (2022).
38. Thornhill, G. D. *et al.* Effective radiative forcing from emissions of reactive gases and aerosols – a multi-model comparison. *Atmospheric Chemistry and Physics* **21**, 853–874 (2021).
39. Eide, M. S. *et al.* Reducing CO_2 from shipping – do non-CO_2 effects matter? *Atmospheric Chemistry and Physics* **13**, 4183–4201 (2013).
40. Lauer, A., Eyring, V., Hendricks, J., Jöckel, P. & Lohmann, U. Global model simulations of the impact of ocean-going ships on aerosols, clouds, and the radiation budget. *Atmospheric Chemistry and Physics* **7**, 5061–5079 (2007).
41. Kramel, D. *et al.* Global Shipping Emissions from a Well-to-Wake Perspective: The MariTEAM Model. *Environ. Sci. Technol.* **55**, 15040–15050 (2021).
42. Kim, Y.-R., Steen, S., Kramel, D., Muri, H. & Strømman, A. H. Modelling of ship resistance and power consumption for the global fleet: The MariTEAM model. *Ocean Engineering* **281**, 114758 (2023).

43. Seland, Ø. *et al.* Overview of the Norwegian Earth System Model (NorESM2) and key climate response of CMIP6 DECK, historical, and scenario simulations. *Geosci. Model Dev.* **13**, 6165–6200 (2020).
44. Dijkstra, E. W. A note on two problems in connexion with graphs. *Numer. Math.* **1**, 269–271 (1959).
45. Kim, Y., Steen, S. & Muri, H. A novel method for estimating missing values in ship principal data. *Ocean Engineering* **251**, 110979 (2022).
46. Millefiori, L. M. *et al.* COVID-19 impact on global maritime mobility. *Sci Rep* **11**, 18039 (2021).
47. Zis, T. P. V. & Cullinane, K. The desulphurisation of shipping: Past, present and the future under a global cap. *Transportation Research Part D: Transport and Environment* **82**, 102316 (2020).
48. Negro, V., Noussan, M. & Chiaramonti, D. The Potential Role of Ammonia for Hydrogen Storage and Transport: A Critical Review of Challenges and Opportunities. *Energies* **16**, 6192 (2023).
49. Kistner, L., Bensmann, A. & Hanke-Rauschenbach, R. Potentials and limitations of battery-electric container ship propulsion systems. *Energy Conversion and Management: X* **21**, 100507 (2024).
50. McKinlay, C. J., Turnock, S. R., Hudson, D. A. & Manias, P. Hydrogen as a deep sea shipping fuel: Modelling the volume requirements. *International Journal of Hydrogen Energy* **69**, 863–873 (2024).
51. Chen, Y. *et al.* Substantial cooling effect from aerosol-induced increase in tropical marine cloud cover. *Nat. Geosci.* **17**, 404–410 (2024).
52. Twomey, S. The Influence of Pollution on the Shortwave Albedo of Clouds. *J. Atmos. Sci.* **34**, 1149–1152 (1977).
53. Sofiev, M. *et al.* Cleaner fuels for ships provide public health benefits with climate tradeoffs. *Nat Commun* **9**, 406 (2018).
54. Gryspeerdt, E. *et al.* Uncertainty in aerosol–cloud radiative forcing is driven by clean conditions. *Atmospheric Chemistry and Physics* **23**, 4115–4122 (2023).

55. Blichner, S. M., Sporre, M. K., Makkonen, R. & Berntsen, T. K. Implementing a sectional scheme for early aerosol growth from new particle formation in the Norwegian Earth System Model v2: comparison to observations and climate impacts. *Geoscientific Model Development* **14**, 3335–3359 (2021).
56. Frey, L., Bender, F. A.-M. & Svensson, G. Cloud albedo changes in response to anthropogenic sulfate and non-sulfate aerosol forcings in CMIP5 models. *Atmos. Chem. Phys.* **17**, 9145–9162 (2017).
57. Acosta Navarro, J. C. *et al.* Amplification of Arctic warming by past air pollution reductions in Europe. *Nature Geosci* **9**, 277–281 (2016).
58. Fiedler, S. *et al.* Historical Changes and Reasons for Model Differences in Anthropogenic Aerosol Forcing in CMIP6. *Geophysical Research Letters* **50**, e2023GL104848 (2023).

Supplementary Files

This is a list of supplementary files associated with this preprint. Click to download.

- Esfandiarietal.2026SupplementaryInformation.docx